Journal of Experimental Botany, Vol. 61, No. 8, pp. 2071–2081, 2010
doi:10.1093/jxb/erq026 Advance Access publication 1 March, 2010

Journal of Experimental Botany
www.jxb.oxfordjournals.org

RESEARCH PAPER

A model for gas transport in pear fruit at multiple scales

Q. Tri Ho[1,*], Pieter Verboven[1,*], Bert E. Verlinden[2] and Bart M. Nicolaï[1,2]

[1] BIOSYST-MeBioS, Katholieke Universiteit Leuven, Willem de Croylaan 42, B-3001 Leuven, Belgium
[2] Flanders Centre of Postharvest Technology, Katholieke Universiteit Leuven, Willem de Croylaan 42, B-3001 Leuven, Belgium

* To whom correspondence should be addressed. E-mail: pieter.verboven@biw.kuleuven.be; quangtri.ho@biw.kuleuven.be

Received 15 November 2009; Revised 24 January 2010; Accepted 26 January 2010

Abstract

A two-dimensional multiscale gas exchange model was developed to evaluate the effect of ambient conditions, fruit size, and maturity on intracellular O_2 and CO_2 concentrations in pear fruit via computational analysis. The model consists of interconnected submodels that describe the gas exchange at the macroscopic scale of the fruit and the microscopic scale of the cells. The multiscale model resulted in a comprehensive description of gas exchange at different scales. The macroscale model was used to describe the gas exchange of the fruit under controlled atmosphere conditions while corresponding intracellular concentrations of microstructure tissue were computed from the microscale. Ripening of the fruit increased the risk of physiological disorders, since increased respiration resulted in anoxia in the fruit centre even under typical storage conditions.

Key words: anoxia, controlled atmosphere storage, gas transport, multiscale modelling, pear.

Introduction

Exchange of O_2 and CO_2 of plants with their environment is essential for metabolic processes such as photosynthesis and respiration. Gas exchange is caused by differences in gas concentrations between the applied external atmosphere and the internal atmosphere of plant organs. In bulky organs, such as fruits and roots, these gradients exist due to O_2 consumption and CO_2 production during respiration and fermentation (Kader, 1988; Geigenberger *et al.*, 2000; Ho *et al.*, 2008). In developing seeds, the combination of respiration and photosynthesis may cause large gradients in gas concentrations (Rolletschek *et al.*, 2003; Borisjuk and Rolletschek, 2009). In leaves, gradients have been observed due to CO_2 assimilation (Morison *et al.*, 2005; Warren, 2008). In some fruits, such as pears, which are typically stored under controlled atmosphere (CA) condition, anoxia may occur, eventually leading to fermentation, which causes a chain of events ultimately leading to cell death, tissue damage, and commercial loss (Franck *et al.*, 2007). For a better understanding of plant metabolism it is important to quantify the metabolic gas exchange and the effect of the external conditions on the intracellular metabolic gas concentration.

Mathematical modelling is a powerful tool to study the mechanisms of gas transport in plant material. Different approaches to gas transport modelling in plant tissue have been reported, from the macroscale (Mannapperuma *et al.*, 1991; Lammertyn *et al.*, 2003; Ho *et al.*, 2008) to the microscale level (Denison, 1992; Aalto and Juurola, 2002; Ho *et al.*, 2009). In macroscale models, plant material is considered as a continuum, which consists of different interconnected tissues characterized by apparent macroscopic properties of the biological materials (Lammertyn *et al.*, 2003; Ho *et al.*, 2008). Apparent gas transport properties of plant tissue have been determined by measuring gas exchange through small tissue samples (Lammertyn *et al.*, 2001; Schotsmans *et al.*, 2003, Ho *et al.*, 2006*a*, *b*). However, plant tissue has a cellular structure. The microscale topology in which individual cells and intercellular space can be distinguished determines to a large extent gas transport in the tissue (Parkhurst and Mott, 1990; Aalto and Juurola, 2002; Mendoza *et al.*, 2007; Verboven *et al.*, 2008). Plant tissue, therefore, cannot be considered as a real continuum material. Inside plant organs such as the fruits, gas is believed to be transported through intercellular spaces (Mendoza *et al.*, 2007; Verboven *et al.*, 2008). O_2 subsequently permeates through the cellular membrane to the cytoplasm and eventually diffuses in the cytoplasm into the

mitochondria where the respiration takes place. The CO_2 produced essentially follows the reverse path.

A microscale gas transport model has been developed to describe gas transport at the cellular level through the intercellular space and cells (Ho *et al.*, 2009). Although such a model provided detailed predictions of the local microscale gas concentrations, a microscale model that covers microscale gas exchange in the entire fruit is currently not feasible because of the excessive computer resources required to solve such a model on the entire microscale topology.

The multiscale modelling paradigm provides an alternative approach to combine the relative simplicity of continuum-type models defined at the macroscale level with the level of detail models incorporating the microscale features. A multiscale gas transport model is basically a hierarchy of models which describe the gas transport phenomena at different spatial scales (see Fig. 1). These models are coupled via computational analysis, in which the model results relevant to a particular spatial scale are linked to simulations at a different spatial scale. Multiscale modelling has been introduced successfully in material science and geoscience (Regenauer-Lieb and Yuen, 2003; Raghavan and Ghosh, 2004; de Pablo and Curtin, 2007) and is also being recognized as a useful tool for biological applications (Seymour, 2001; Wood *et al.*, 2002, Mebatsion *et al.*, 2008). In this contribution, a multiscale model will be introduced and validated to perform a computational analysis of gas exchange in plant materials at different scales. Pear fruit was chosen as a model system. Since ripening fruit is more susceptible to storage disorder (Veltman *et al.*, 1999; Lammertyn *et al.* 2000; Franck *et al.*, 2003), the model will be applied to evaluate the effect of environmental conditions, fruit size, and maturity on cellular respiration and the risk of local fermentative conditions.

Materials and methods

Materials

Pears (*Pyrus communis* 'Conference') were harvested on 20 August 2007, at the pre-climacteric stage at the Fruitteeltcentrum (Rillaar, Belgium), cooled, and stored according to commercial protocols for a period of 21 d at –1 °C followed by CA storage (2.5 kPa O_2, 0.7 kPa CO_2 at –1 °C) until they were used for the experiments. These fruit were considered as the control treatment and will be further designated as 'control fruit'; some fruit were stored for another 7 d at 20 °C in ambient air as a ripening treatment and will be designated as 'ripe fruit'.

Continuum model of gas exchange in intact fruit

At the macroscopic spatial scale, the fruit tissue was considered as a continuum of material. A permeation–diffusion–reaction model (Ho *et al.*, 2008) was applied to study gas exchange due to respiration of intact fruit with the environment:

$$\alpha_i \frac{\partial C_i}{\partial t} + \nabla \cdot (\mathbf{u} C_i) = \nabla \cdot D_i \nabla C_i + R_i \quad (1)$$

$$C_i = C_{i,\infty} \quad (2)$$

where α_i is the gas capacity of component i in the tissue and C_i (mol m^{-3}) is the concentration of gas i (O_2, CO_2, N_2). In the equations, D_i (m^2 s^{-1}) is the apparent diffusion coefficient, $\mathbf{u}$ (m s^{-1}) the apparent velocity vector, R_i (mol m^{-3} s^{-1}) the production term of the gas component i related to O_2 consumption or CO_2 production, and t (s) the time. The index ∞ refers to the gas concentration of the ambient atmosphere.

Gas partial pressure gradients were considered to be the driving force for diffusive gas transport. Differences in diffusion rates of

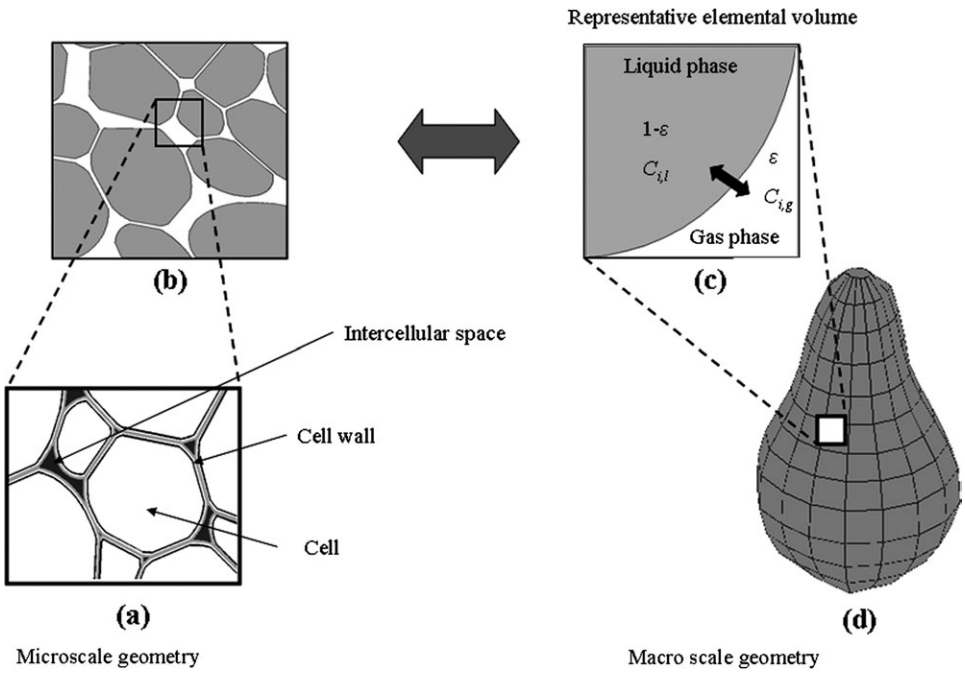

Fig. 1. Multiscale hierarchy of pear geometry. (a) Detailed microstructure of tissue; (b) and (c) tissue and its representative elemental volume; (d) pear geometry. $C_{i,g}$ and $C_{i,l}$ are concentration of gas i in the gas and liquid phase while ϵ is the porosity of tissue.

the different gases led to total pressure gradients that caused convective exchange as described by Darcy's law.

$$\mathbf{u} = -\frac{K}{\mu}\nabla P = -\frac{K.R.T}{\mu}\nabla\left(\sum C_i\right) \quad (3)$$

with K (m^2) the permeation coefficient, P (Pa) the pressure, and μ (Pa.s) the viscosity of the gas. The relationship between the gas concentration and pressure was assumed to follow the ideal gas law ($P=CRT$).

The extended Michaelis–Menten kinetics have been applied as a semi-empirical model to describe the respiration characteristic of intact and tissue fruit (Peppelenbos *et al.*, 1996; Hertog *et al.*, 1998; Lammertyn *et al.*, 2001*b*; Ho *et al.*, 2008). A non-competitive inhibition model was used to describe O_2 consumption as formulated by Equation 4:

$$R_{O_2} = -\frac{V_{m,O_2}.C_{O_2}}{\left(K_{m,O_2}+C_{O_2}\right).\left(1+\frac{C_{CO_2}}{K_{mn,CO_2}}\right)} \quad (4)$$

with V_{m,O_2} (mol m^{-3} s^{-1}) the maximum oxygen consumption rate, C_{O_2} (mol m^{-3}) the O_2 gas concentration, C_{CO_2} (mol m^{-3}) the CO_2 gas concentration, K_{m,O_2} (mol m^{-3}) the Michaelis–Menten constant for O_2 consumption, K_{mn,CO_2} (mol m^{-3}) the Michaelis–Menten constant for non-competitive CO_2 inhibition, and R_{O_2} (mol m^{-3} s^{-1}) the O_2 consumption rate of the sample. The equation for the production rate of CO_2 consists of an oxidative respiration part and a fermentative part.

$$R_{CO_2} = -r_{q,ox}.R_{O_2} + \frac{V_{m,f,CO_2}}{\left(1+\frac{C_{O_2}}{K_{m,f,O_2}}\right)} \quad (5)$$

with V_{m,f,CO_2} (mol m^{-3} s^{-1}) the maximum fermentative CO_2 production rate, K_{m,f,O_2} (mol m^{-3}) the Michaelis–Menten constant of O_2 inhibition on fermentative CO_2 production, $r_{q,ox}$ the respiration quotient at high O_2 partial pressure, and R_{CO_2} (mol m^{-3} s^{-1}) the CO_2 production rate of the sample. The effect of temperature on the respiration rate was described by Arrhenius' law (Hertog *et al.*, 1998).

The macroscale geometrical model was based on reconstructed photographic images of intact pear. The pear geometry was considered to be axi-symmetric and the model was solved with gas concentration variations in the radial direction (r) and vertical axis (z). To study the effect of fruit size on gas exchange, geometrical models were constructed with radii of 2.6, 3, 3.2, 3.7, and 4.2 cm by scaling the original geometrical model. The model was solved using the finite element method (Comsol 3.3, Comsol AB, Stockholm, Sweden).

Gas transport parameters: The gas exchange properties of the fruit tissue were measured in the measurement set-up using fluorescent optical probes. The system consisted of two chambers (measurement chamber and flushing chamber) separated by the disc-shaped tissue sample. Due to different applied gas concentrations between the two chambers, gas diffusions took place. The O_2 and CO_2 concentrations were measured in the measurement chamber with fluorescent optical probes (Foxy-Resp and FCO2-R; Ocean Optics). The gas diffusion properties were then estimated from the gas concentration profiles as described by Ho *et al.* (2006*a*). The N_2 diffusivity was determined indirectly from the total pressure and the O_2 partial gas pressure of the binary O_2–N_2 gas mixture (Ho *et al.*, 2006*b*).

Permeation properties of pear epidermis and cortex tissue were determined by measuring the total pressure difference between two chambers separated by a tissue sample (Ho *et al.*, 2006*b*). Both chambers were flushed with humidified N_2 gas at 10.0 l h^{-1}. The pressure was adjusted so as to obtain a 6 kPa pressure difference between the measurement and flushing chamber. The inlet and outlet valves of one chamber were closed, and the decrease in pressure of this chamber was monitored for at least 4 h. The permeability was then estimated from this pressure drop using the procedure described by Ho *et al.* (2006*b*). More details can be found in Ho *et al.* (2006*a*, *b*).

Respiration kinetic parameters: A non-competitive inhibition model was used to describe respiration kinetics of fruit tissue. Respiration kinetic parameters were reported by Ho *et al.* (2008). The respiratory activity of pear depends on its maturity (Veltman *et al.*, 1999). Since the respiration rate was assumed to be determined by one rate-limiting enzymatic reaction (Chevillotte, 1973), the Michaelis–Menten constant $K_{m,c}$, which is a ratio of rate constants, would be expected to be relatively independent of temperature (Hertog *et al.*, 1998). The K_m value for O_2 and CO_2 was therefore assumed to be constant and was taken from Ho *et al.* (2008) (see Table 2). On the other hand, the maximal O_2 consumption rate V_{m,O_2} and maximal CO_2 fermentative production rate V_{m,f,CO_2} are a function of the initially available enzyme concentration (Hertog *et al.*, 1998). These parameters were, therefore, considered to vary from batch to batch, depending on fruit maturity and season. To determine the V_{m,O_2} and V_{m,f,CO_2} values of tissue, a respiration experiment was carried out in which a pear was put into a closed jar in ambient air at –1 °C.

Each 1.7 l jar containing two pear fruits resulted in ~224 g pear l^{-1}. Two different air conditions were applied at 20 kPa O_2, 0 kPa CO_2, and 0 kPa O_2, 0 kPa CO_2 by gas mixtures. The gas mixtures were made from pure gases using an in-house built mixing panel equipped with mass flow controllers (Brooks Instrument, The Netherlands). The composition of the mixtures was measured by using a gas analyser (Checkmate II, PBI Dansensor, Denmark) and the resultant accuracy of the concentration in the mixture was better than 0.2 kPa from the reading of the gas analyser. The gas analyser has an accuracy of ±0.1% absolute for the O_2 reading and ±0.5% absolute for the CO_2 reading, and was calibrated against calibrated mixtures (Air products N.V., USA). For each of conditions, three jars were connected in series and flushed with conditioned air for at least 1 d. Then the jars were closed and the O_2 and CO_2 gas partial pressure changes with time were measured by the gas analyser. The gas percentages were converted to partial pressures by multiplying them by the measured total pressure (DPI 142, GE Druck, Germany). V_{m,O_2} and V_{m,f,CO_2} were estimated by fitting the macroscale model to the experimental data using a non-linear least squares estimation program written in Matlab (The Mathworks, Inc., Natick, USA). To determine the changes of V_{m,O_2} and V_{m,f,CO_2} due to ripening, the pears were kept for a period of 7 d at 20 °C in normal air preceding the respiration measurement at –1 °C. Then, the V_{m,O_2} and V_{m,f,CO_2} of tissue were estimated based on the respiration measurement data.

Microscale model

The microscale model was applied to describe respiratory gas diffusion in the intercellular space (pore), the cell wall network, and through the cell membrane into the cytoplasm (Ho *et al.*, 2009). For the intracellular liquid phase, gas diffusion in the liquid was coupled to cellular respiration kinetics.

O_2 transport model: Microscale diffusion was assumed to dominate transport through each of the compartments and was described by Fick's second law, with the characteristic diffusion coefficient D_{O_2} (Eq (6)). Respiration was incorporated into the model as a source term R_{O_2}.

$$\frac{\partial C_{O_2}}{\partial t} = \nabla\cdot D_{O_2}\nabla C_{O_2} + R_{O_2} \quad (6)$$

where C_{O_2} (mol m^{-3}) is the O_2 concentration in a certain phase and D_{O_2} (m^2 s^{-1}) is the O_2 diffusivity. The relationship between the O_2 concentration in the gas phase $C_{O_2,g}$ and that in the liquid phase $C_{O_2,l}$ is given by Henry's law:

$$C_{O_2,l} = R \cdot T \cdot H_{O_2} \cdot C_{O_2,g} \quad (7)$$

with R (8.314 J mol^{-1} K^{-1}) the universal gas constant, T (K) the temperature, and H_{O_2} (mol m^{-3} kPa) Henry's constant for O_2. In the intracellular liquid phase, Michaelis–Menten kinetics were used as a phenomenological model to describe the O_2 consumption rate of cell protoplasts (Lammertyn *et al.*, 2001*b*):

$$R_{O_2} = -\frac{V_{m,O_2} \cdot C_{O_2}}{K_{m,O_2} + C_{O_2}} \quad (8)$$

with V_{m,O_2} (mol m^{-3} s^{-1}) the maximum oxygen consumption rate in the liquid phase and K_{m,O_2} (mol m^{-3}) the Michaelis–Menten constant for O_2 consumption. The cell membrane is essentially a phospholipid bilayer. Passive gas transfer across the cell membrane occurs according to Fick's first law as a consequence of a concentration difference over the membrane. The flux J_{O_2} (mol m^{-2} s^{-1}) through the membrane was equal to

$$J_{O_2} = -h_{O_2,mem} \Delta C_{O_2} = -h_{O_2,mem} \left(C_{O_2} - C^*_{O_2} \right) \quad (9)$$

where $h_{O_2,mem}$ (m s^{-1}) is the O_2 permeability of the cell membrane and $C^*_{O_2}$ mol m^{-3} is the equilibrium O_2 concentration in the liquid phase of the outer membrane.

CO_2 transport model: For pores and cell walls, the following equation was used:

$$\frac{\partial C_{CO_2}}{\partial t} = \nabla \cdot D_{CO_2} \nabla C_{CO_2} \quad (10)$$

where C_{CO_2} (mol m^{-3}) is the CO_2 concentration in a certain phase and D_{CO_2} (m^2 s^{-1}) is the CO_2 diffusivity. The model of CO_2 transport in the liquid phase was

$$\frac{\partial C_{CO_2}}{\partial t} = \nabla \cdot D_{CO_2} \nabla C_{CO_2} + R_{CO_2} - k_1 C_{CO_2} + k_2 \frac{[H]^+ C_{HCO_3^-}}{K} \quad (11)$$

$$\frac{\partial C_{HCO_3^-}}{\partial t} = \nabla \cdot D_{HCO_3^-} \nabla C_{HCO_3^-} + k_1 C_{CO_2} - k_2 \frac{[H]^+ C_{HCO_3^-}}{K} \quad (12)$$

with $C_{HCO_3^-}$ (mol m^{-3}), $D_{HCO_3^-}$ (m^2 s^{-1}) the cytoplasmic concentration and diffusivity of HCO_3^-, respectively, R_{CO_2} (mol m^{-3} s^{-1}) the cytoplasmic CO_2 production rate, and k_1 (s^{-1}) and k_2 (s^{-1}) the CO_2 hydration rate constant and H_2CO_3 dehydration rate constant, respectively. $[H]^+$ (mol L^{-1}) and K (mol L^{-1}) are the concentration of protons H^+ and the acid dissociation constant for H_2CO_3. A more detailed explanation can be found in Ho *et al.* (2009). The latter two terms of Equations 11 and 12 represent the forward and backward conversion rate of CO_2 to HCO_3^-, respectively. The equation for the production rate of CO_2 in the cytoplasm accounts for both oxidative and fermentative respiration.

$$R_{CO_2} = -r_{q,ox} . R_{O_2} + \frac{V_{m,f,CO_2}}{\left(1 + \frac{C_{O_2}}{K_{m,f,O_2}}\right)} \quad (13)$$

The first term on the right hand side indicates the oxidative CO_2 production rate due to consumption of O_2; the second term represents anoxic conditions in the cell where the oxidative respiration process is inhibited and replaced by a fermentation pathway.

Similar to O_2 transport, the flux J_{CO_2} (mol m^{-2} s^{-1}) through the membrane was written as

$$J_{CO_2} = -h_{CO_2,mem} \Delta C_{CO_2} = -h_{CO_2,mem} \left(C_{CO_2} - C^*_{CO_2} \right) \quad (14)$$

with V_{m,f,CO_2} (mol m^{-3} s^{-1}) the maximum fermentative CO_2 production rate of the intracellular cellular liquid phase, K_{m,f,O_2} (mol m^{-3}) the Michaelis–Menten constant of O_2 inhibition on fermentative CO_2 production, and $r_{q,ox}$ the respiration quotient at high O_2 partial pressure (the ratio between CO_2 production and O_2 consumption). The relationship between the equilibrium CO_2 concentration in the gas and liquid phase was again assumed to be described by Henry's law:

$$C_{CO_2,l} = R \cdot T \cdot H_{CO_2} \cdot C_{CO_2,g} \quad (15)$$

with H_{CO_2} (mol m^{-3} kPa^{-1}) Henry's constant for CO_2.

Parameters of the microscale were reported by Ho *et al.* (2009) (see Supplementary Table S1 available at *JXB* online). The V_{m,O_2} of tissue was converted to the value for cytoplasm by dividing it by the porosity of the tissue.

Tissue geometries were constructed from light microscopic images of cortex parenchyma tissue of pear and generated using the ellipse tessellation algorithm (Mebatsion *et al.*, 2006). The tissue model was then imported into a finite element simulation code (Comsol 3.3, Comsol AB, Stockholm, Sweden) via a Matlab interface (see more details in Mebatsion *et al.*, 2006) where a finite element mesh was generated on the pear geometry. Equations of gas exchange were discretized over the meshed geometry and solved using the finite element method in Comsol.

Multiscale model and localization

In this computational analysis for multiscale simulation, the macroscale gas transport model was first applied to predict the respiratory gas distribution in the fruit. Simulations were carried out for pears under well-defined environmental conditions. In total, 35 conditions, ranging from 0.1 kPa to 3.5 kPa O_2 in combination with 0.7 kPa CO_2 at –1 °C were applied. The critical region was defined as the position where the O_2 and CO_2 concentrations in the pear were minimal and maximal, respectively, as predicted by the macroscale model. This region was considered to be likely to switch to a fermentative metabolism due to anoxia or high CO_2 partial pressure. The microscale model was solved to compute the corresponding intracellular concentration. Hence, the gas concentration of the critical region of the macroscale model was applied at the boundary of the computational domain in the microscale simulation. The model was solved by means of the finite element method in Comsol Multiphysics vs. 3.3 (Comsol AB, Stockholm).

Results

Macroscale model, gas exchange properties, and respiration kinetics parameters

The measured gas transport properties are shown in Table 1. A high variability was observed. The gas diffusivity values of the epidermis and subepidermis were small. The higher diffusivity in the axial direction compared with that in the radial direction is probably due to the fact that vascular bundles are not filled with sap during storage of the fruit and thus can be considered as hollow tubes facilitating gas transport (Verboven *et al.*, 2008). It is likely, therefore, that the vascular bundles along the axis of the pear indeed facilitate gas exchange. The diffusivity of CO_2 was larger than that of O_2 and N_2.

An extended Michaelis–Menten kinetics model was applied to the respiration submodel of the macroscale. The Michaelis–Menten constants were assumed not to depend on temperature and were taken from Ho *et al.* (2008). Only the maximal O_2 consumption rate V_{m,O_2} and maximal CO_2 fermentative production rate V_{m,f,CO_2} were assumed to vary depending on fruit maturity and differ from batch to batch.

These parameters were determined by fitting the macroscale model prediction to the measured respiration kinetics of intact fruit. The fit is shown in Fig. 2. The estimated values of V_{m,O_2} and V_{m,f,CO_2} of tissue for ripe fruit measured at –1 °C following storage for 7 days at 20 °C in ambient air were considerably larger than those for the control fruit (see Table 3).

The macroscale model parameters were validated by comparing the measured O_2 and CO_2 concentration as a function of time in the jar with simulated values at 10 °C. A good agreement between simulations and measurements was observed, as depicted in Fig. 3.

A simulation result of the respiratory gas distribution inside the fruit under low oxygen conditions is shown in Fig. 4. Due to the diffusion barrier, a concentration gradient was found inside the pear. A decrease of O_2 partial pressure and an increase of CO_2 partial pressure inside the fruit were observed. Ripening of the fruit increased the respiration, leading to much lower levels of oxygen in the centre of fruit compared with the control fruit (Fig. 4b).

Table 1. Estimated gas diffusion properties of the macroscale gas transport model and their 95% confidence interval

The number of replicates varied between six and eight. Skin was defined here as the combination of epidermis and hypodermis.

Parameter	Units	Estimated value
D_{O_2},skin	$m^2\ s^{-1}$	$(1.86\pm0.70)\times10^{-10}$ [a]
D_{CO_2},skin	$m^2\ s^{-1}$	$(5.06\pm3.3)\times10^{-10}$ [a]
D_{N_2},skin	$m^2\ s^{-1}$	$(1.06\pm0.29)\times10^{-10}$ [b]
K_{skin}	m^2	$(2.17\pm1.43)\times10^{-19}$ [b]
D_{O_2},r	$m^2\ s^{-1}$	$(5.63\pm3.09)\times10^{-10}$
D_{CO_2},r	$m^2\ s^{-1}$	$(5.32\pm1.43)\times10^{-9}$
D_{N_2},r	$m^2\ s^{-1}$	$(6.3\pm3.7)\times10^{-10}$
K_r	m^2	$(6.23\pm8.25)\times10^{-19}$
D_{O_2},z	$m^2\ s^{-1}$	$(3.18\pm1.3)\times10^{-9}$
D_{CO_2},z	$m^2\ s^{-1}$	$(1.4\pm4.3)\times10^{-8}$
D_{N_2},z	$m^2\ s^{-1}$	$(1.66\pm1.11)\times10^{-9}$
K_z	m^2	$(9.8\pm13.0)\times10^{-17}$

[a] Values measured by Ho *et al.* (2006*a*).
[b] Values measured by Ho *et al.* (2006*b*).

Microscale gas exchange model

The microscale gas exchange model was applied to the intercellular space (pore), the cell wall network, the cell membrane, and the cytoplasm (Ho *et al.*, 2009). The microscale gas exchange was validated by comparing the macroscopic apparent diffusivity computed from the microscale with the measurement (see Table 4). In addition, good agreement was found between simulated macroscopic gas concentration gradients and the microscale model (Ho *et al.*, 2009). The simulated intracellular O_2 concentration computed in the critical region (lowest O_2 concentration) of the macroscale fruit is shown in Fig. 5. Heterogeneity of intracellular concentrations was found. The results show that the intracellular O_2 concentration of the control fruit was much higher than that of the ripe fruit.

Multiscale modelling of gas exchange in relation to environmental conditions

In this computational analysis for multiscale gas exchange, the continuum model was first simulated with different external conditions and fruit sizes at a storage temperature of –1 °C. The critical region is defined as the site where the lowest O_2 and highest CO_2 were computed from the macroscale model. Then, the intracellular level was analysed by simulating gas transport using the microscale model with boundary conditions from the critical values of the macroscale simulation. The results showed that the difference between the lowest concentration of the cells computed from the microscale model and that estimated by the macroscale model of the normal pear at –1 °C ranged from 1.3% to 6.2% under ultra low O_2 conditions. The corresponding minimal O_2 concentration (μM) in the cytoplasm as a function of external O_2 partial pressure and pear radius is shown in Fig. 6. The minimal O_2 concentration increased with increasing external O_2 partial pressure and decreased with increasing radius. With a typical external O_2 partial pressure of 2.5 kPa, the minimal O_2 concentration for the fruit with radius from 2.6 cm to 4.2 cm was >1 μM.

To study the effect of fruit ripening on the risk of storage disorder development, the measured maximal O_2 consumption rate V_{m,O_2} and maximal CO_2 production rate V_{m,f,CO_2}

Table 2. Respiration kinetic parameters of the macroscale gas transport model

Parameters	Units	Estimated values[a]
Maximal O_2 consumption rate of tissue V_{m,O_2},tissue (–1 °C)	$mol\ m^{-3}\ s^{-1}$	$(1.1173\pm0.0003)\times10^{-5}$
Maximal fermentative CO_2 production rate of tissue V_{m,f,CO_2},tissue (–1 °C)	$mol\ m^{-3}\ s^{-1}$	$(1.1148\pm0.0002)\times10^{-5}$
Activation energy of O_2 consumption E_{a,VmO_2}	$kJ\ mol^{-1}$	80.2 ± 12.3 [b]
Activation energy of CO_2 production $E_{a,VmfCO_2}$	$kJ\ mol^{-1}$	56.7 ± 13.3 [b]
Michaelis–Menten constant for O_2 consumption K_{m,O_2}	kPa	1.00 ± 0.23 [b]
Michaelis–Menten constant for non-competitive CO_2 inhibition K_{mn,CO_2}	kPa	66.4 ± 21.3 [b]
Michaelis–Menten constant of O_2 inhibition on fermentative CO_2 production K_{m,f,O_2}	kPa	0.28 ± 0.14 [b]
Respiration quotient $r_{q,ox}$		0.83 ± 0.0004

[a] ± 95% confidence limits.
[b] Parameters were taken from Ho *et al.* (2008). The other parameters were estimated by fitting the macroscale model to the measured O_2 and CO_2 gas partial pressures in the jars.

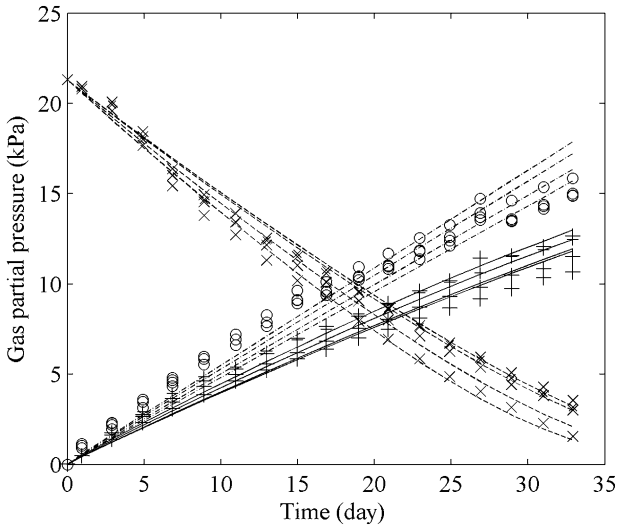

Fig. 2. O_2 and CO_2 concentration as a function of time in a closed jar at a storage temperature of –1 °C. Dashed lines and solid lines indicate the O_2 and CO_2 partial pressure in jars fitted by the permeation–diffusion–reaction model. The symbols (×) and (+) indicate the measured O_2 and CO_2 gas partial pressure. The initial condition was set to 20 kPa O_2, 0 kPa CO_2. The dash-dotted line and open circles indicate the simulated and measured CO_2 gas partial pressure in the jar with an initial condition of 0 kPa O_2, 0 kPa CO_2. Under these conditions the O_2 partial pressure obviously remained equal to 0 kPa.

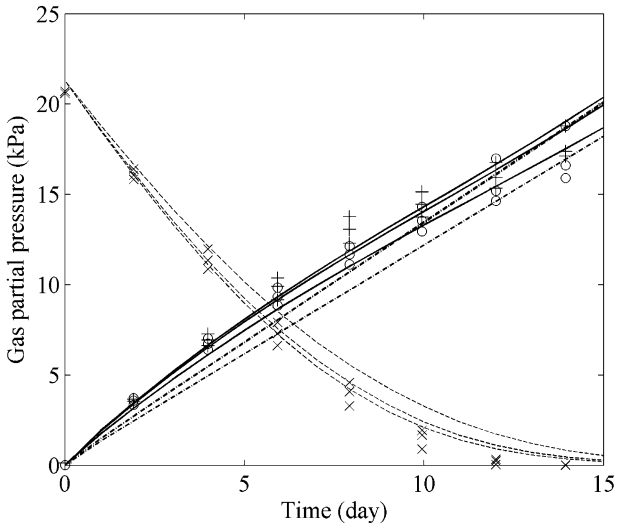

Fig. 3. Validated O_2 and CO_2 concentration as a function of time in a closed jar at a storage temperature of 10 °C. Dashed lines and solid lines indicate the O_2 and CO_2 partial pressure in jars predicted by the permeation–diffusion–reaction model. The symbols (×) and (+) indicate the measured O_2 and CO_2 gas partial pressure. The initial condition was set to 20 kPa O_2, 0 kPa CO_2. The dash-dotted line and open circles indicate the simulated and measured CO_2 gas partial pressure in the jar with an initial condition of 0 kPa O_2, 0 kPa CO_2. Under these conditions the O_2 partial pressure obviously remained equal to 0 kPa.

Table 3. Maximal O_2 consumption rate V_{m,O_2}, and maximal CO_2 production rate V_{m,f,CO_2} of tissue

The values were estimated by fitting the permeation–diffusion–reaction model to the measured data.

Respiration	Maximal O_2 consumption rate of tissue V_{m,O_2},tissue (mol m^{-3} s^{-1})	Maximal CO_2 production rate of tissue V_{m,f,CO_2},tissue (mol m^{-3} s^{-1})
At –1 °C	1.12×10^{-5}	1.11×10^{-5}
Effect of ripening[a]	2.93×10^{-5}	3.57×10^{-5}

[a] Pear stored at 20 °C for 7 d for ripening, then again at –1 °C.

of tissue due to ripening (Table 3) were used for the macroscale simulation. The microscale model was used to predict the corresponding intracellular concentration at the critical region from the macroscale model. The difference between the lowest concentration of the cells computed from the microscale model and that estimated by the macroscale model of the ripening pear at –1 °C ranged from 11.4% to 14% under ultra low O_2 conditions. The simulated minimal O_2 concentration (μM) in the cytoplasm at –1 °C is shown in Fig. 6. The results demonstrate that the increasing respiration rate due to fruit ripening may lead to anoxia in storage. The multiscale model indicated that the minimal O_2 concentration in ripe fruit was more severe compared with that of control fruit. While control fruit had a minimal O_2 concentration >1 μM, in ripe and large fruit this value decreased to <0.1 μM with an external O_2 partial pressure of 2.5 kPa.

The maximal CO_2 concentration in the centre of the fruit was computed for different pear radii and ambient O_2 concentrations. The CO_2 concentration in the centre of the fruit is more sensitive to the fruit size (Fig. 7). In small fruit (R_{pear} <3 cm), the CO_2 concentration seemed to be saturated with increasing O_2 concentration. Increasing the fruit size led to a high CO_2 concentration in the centre of the fruit.

Discussion

Pear fruit are commercially stored at low temperature under CA conditions to retard physiological processes in the fruit by decreasing the O_2 partial pressure and by increasing the CO_2 partial pressure. However, the optimal gas composition is critical, as too low an O_2 partial pressure can induce fermentative metabolism in the fruit (Beaudry, 1999). In other organs, gas availability is also critical. In seeds, oxygen falls to very low levels inside developing embryos (Rolletschek *et al.*, 2002) and maintains a minimum level which has been shown to affect the overall rate of metabolism. Anoxia stress may lead to hydrogen peroxide formation in plant cells and be harmful for cellular metabolic processes (Blokhina *et al.*, 2001). The gas exchange model may be useful to predict the internal gas concentration coupled to metabolic processes, to optimize plant metabolism by changing the oxygen availability.

Cytochrome *c* oxidase has been considered as the rate-limiting enzyme in the oxidative respiration pathway

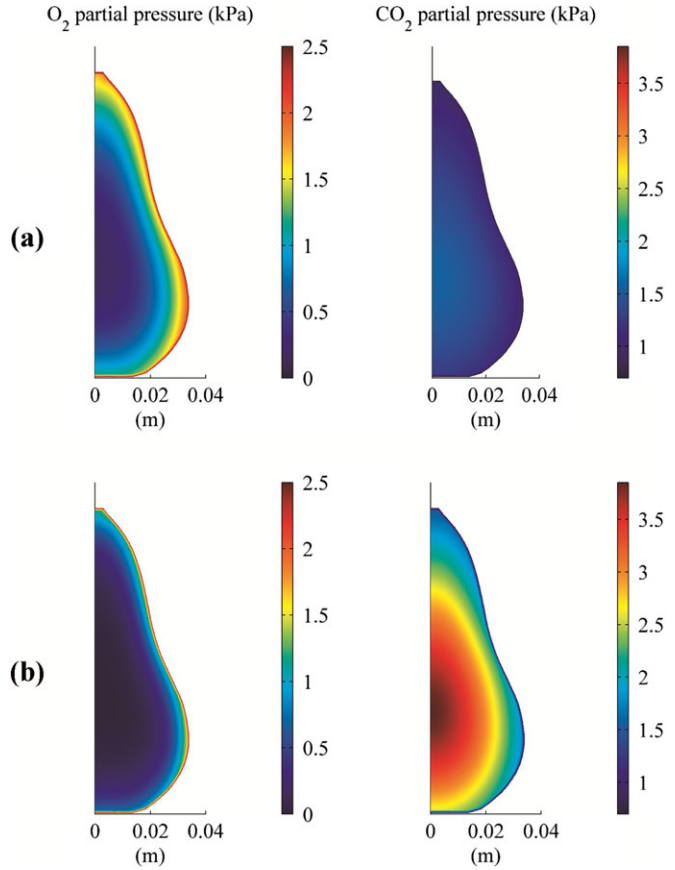

Fig. 4. O_2 and CO_2 distribution of the intact fruit under typical commercial storage conditions (2.5 kPa O_2, 0.7 kPa CO_2 and –1 °C); (a) control fruit, (b) ripe fruit.

Table 4. Macroscopic apparent diffusivity of O_2 and CO_2 in pear parenchyma tissue (Ho *et al*., 2009)

The values reported for the microscale model are average values for nine different tissue geometries.

	T (°C)	$D_{CO_2 tissue}$ ($m^2\ s^{-1}$)[a]	$D_{CO_2 tissue}$ ($m^2\ s^{-1}$)
Microscale model	20	$(3.54\pm0.68)\times10^{-10}$	$(3.13\pm0.59)\times10^{-9}$
	0	$(3.23\pm0.63)\times10^{-10}$	$(2.83\pm0.45\times10^{-9}$
Measurement	20	$(2.87\pm0.45)\times10^{-10}$[a]	$(2.6\pm0.36)\times10^{-9}$[b]
	12	$(4.3\pm1.7)\times10^{-10}$[c]	$(1.73\pm1.15)\times10^{-9}$[c]
	20	$(5.63\pm3.09)\times10^{-10}$[d]	$(5.32\pm1.43)\times10^{-9}$[d]

[a] ± 95% confidence limits.
[b] Ho *et al.* (2006*a*).
[c] Schotsmans *et al.* (2003).
[d] Present experiment (Ho *et al.*, 2009).

(Chevillotte, 1973). Ludwig *et al.* (2001) considered that oxidative respiration was controlled by cytochrome *c* oxidase activity and ATP synthase. From 80% to 90% of the oxygen consumed by an organism is believed to be reduced to water by cytochrome *c* oxidase, the terminal enzyme of the respiratory chain (Rolfe and Brown, 1997; Gnaiger, 2003). Different values for K_{m,O_2} of cytochrome *c* oxidase were found in the literature. Solomos (1982) obtained a value of 0.1 μM for the K_{m,O_2} of isolated cytochrome *c* oxidase for apple. Millar *et al.* (1994) calculated a K_{m,O_2} value of 0.14 μM in soybean shoot mitochondria, while Taiz and Zeiger (1993) found a K_{m,O_2} value of 1 μM for the cytochrome *c* oxidase in plant tissue. The computational analysis presented here revealed that the O_2 concentration of control fruit stored at typical CA conditions (2.5 kPa O_2, 0.7 kPa CO_2 at –1 °C) was higher than the Michaelis–Menten constant for cytochrome *c* oxidase $K_{m,c}$, the rate-limiting enzyme of the respiration pathways. Consequently, the respiratory pathway will be active with O_2 supply. In contrast to small pears, in large pears and under extremely low O_2 storage conditions the oxygen concentration can decrease well below the Michaelis–Menten constant for cytochrome *c* oxidase. This most probably leads to anoxia, and physiological disorders have been observed under such conditions (Lammertyn *et al.*, 2000).

Ripening of the fruit increases the risk of physiological disorders because increasing the respiration rate due to ripening resulted in anoxia in the central region of the fruit even under typical CA conditions (Fig. 6). Depletion of O_2 in the sensitive region was more severe in large fruit compared with small fruit. This corresponds to the observation that late picked fruit was more susceptible to storage disorders described by Lammertyn *et al.* (2000). This is a major step forward in understanding the biophysical processes underlying physiological disorders compared with statistical models such as that developed by Lammertyn *et al.* (2000).

The internal gas partial pressures, which depend on the externally applied gas partial pressures and gas transport properties of the fruit, influence the respiration rate and, hence, the intracellular energy level (Saquet *et al.*, 2003), as well as the antioxidant system (Agar *et al.*, 1997; Veltman *et al.*, 1999; Larrigaudiere *et al.*, 2001; Franck *et al.*, 2003, 2007). It was found here that CO_2 does not have a clear effect on the pear respiration rate (the value of K_{mn,CO_2} is indeed very high). Similar results were also found by Peppelenbos and Van't Leven (1996) for Goldon Delicious apple, Elstar apple, and asparagus. However, an effect of CO_2 was found for broccoli, mungbean sprouts, and cut chicory. There is no clear reason why there should be such a difference; in fact, relatively little is known about the effect of CO_2 on the activity of respiratory enzymes. However, a high CO_2 partial pressure during storage of the fruit was likely to induce brown core development in Conference pears (Veltman *et al.*, 1999; Franck *et al.*, 2003, 2007). Note that the pH of the cytoplasm is controlled by the pH buffering capacity (Smith and Raven, 1979; Boron, 2004) and proton pumps (Nishi and Forgac, 2002); the required ATP energy for the proton transport is provided by the V-ATPases system (Nishi and Forgac, 2002). Increasing the CO_2 level in the pore of fruit tissue may lead to a decreased pH in the cytoplasm. To maintain the pH of the cytoplasm, the intracellular system may need more energy for pumping of protons among the compartments. Shortage of energy could then occur during storage of the fruit to maintain the intracellular pH at high CO_2 concentration levels. Moreover, it is possible that a change in the pH may result in loss of the membrane integrity and formation of reactive oxygen species such as superoxide species during respiration. This may

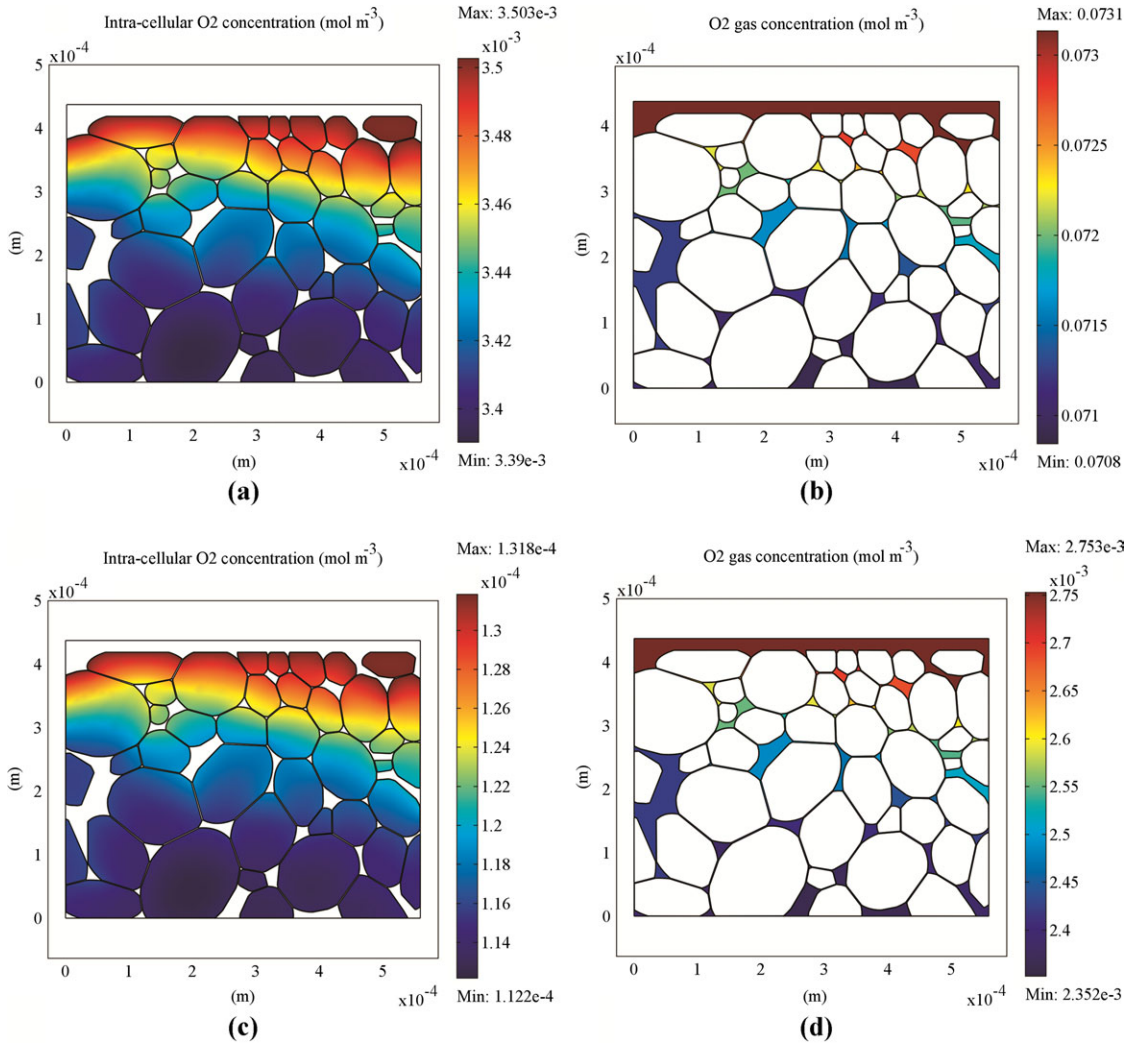

Fig. 5. The simulated intracellular O_2 concentration (μM) of microscopic tissue. (a) and (c) The intracellular O_2 concentration of control and ripe fruit. (b) and (d) O_2 concentration in the gas phase of control and ripe fruit computed from the critical region (lowest O_2 concentration) of the macroscale simulation.

explain the impairment of the anti-oxidation system (L-ascorbic acid distribution) and brown core development in pear, as was found in the literature (Veltman *et al.*, 1999, 2003; Franck *et al.*, 2003, 2007; Saquet *et al.*, 2003).

The modified Michaelis–Menten kinetics which are now included in the multiscale gas exchange model are incapable of predicting such detailed biochemical information. This kinetic model needs to be updated by a new and more comprehensive model which should describe the pathways of respiration and fermentation.

Conclusions

A multiscale model was developed to study the effect of ambient air composition on gas exchange of fruit during commerical storage. A computational study revealed that oxidative respiration can be still active at typical CA conditions (2.5 kPa O_2, 0.7 kPa CO_2 at –1 °C) since the O_2 concentration inside control fruit stored was higher than the Michaelis–Menten constant for cytochrome *c* oxidase $K_{m,c}$, the rate-limiting enzyme of the respiration pathway. In contrast to small pears, in large pears and under very low O_2 storage conditions the oxygen concentration can decrease well below the Michaelis–Menten constant for cytochrome *c* oxidase. This most probably leads to fermentation and physiological disorders which have been observed under such conditions. Ripening of the fruit causes an increased risk of physiological disorders since increasing the respiration rate due to ripening resulted in anoxia in the cental region of the fruit even under commercial CA conditions. A multiscale approach can provide a much better insight into the mechanism of gas exchange in pear and in fruit tissue in general, and for the first time a quantitative explanation of the relationship between gas exchange and the development of physiological disorders in fruit has been provided.

Supplementary data

Supplementary data are available at *JXB* online.

Table S1 Physical parameters of the microscale gas transport model (Ho *et al.*, 2009).

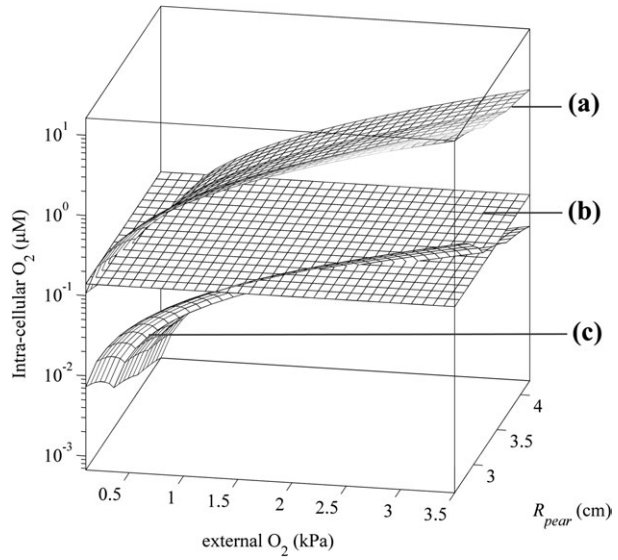

Fig. 6. The intracellular O_2 concentration (μM) of the critical region as a function of O_2 partial pressure and pear radius. The storage temperature was –1 °C. (a) Control fruit; (b) O_2 concentration that is equal to the Michaelis–Menten constant for cytochrome *c* oxidase $K_{m,c}$ (0.14 μM) (Millar *et al.*, 1994); (c) ripe fruit.

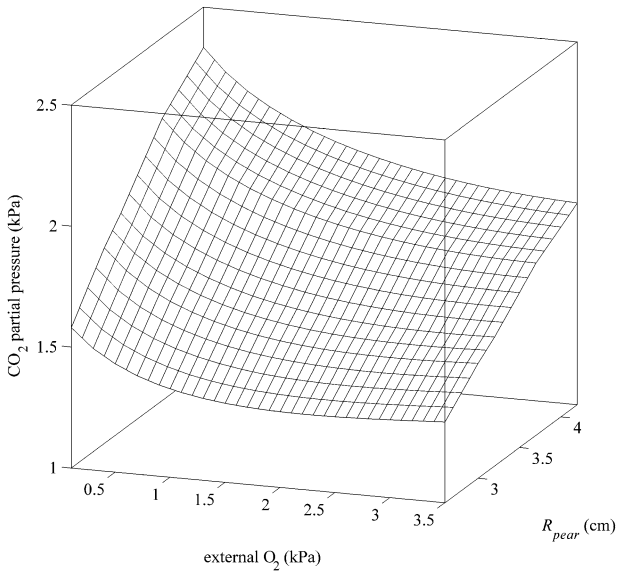

Fig. 7. Maximal CO_2 concentration (kPa) computed from the macroscale model of control fruit as a function of O_2 partial pressure and pear radius. The storage temperature was –1 °C.

Acknowledgements

The authors wish to thank the Research Council of the KU Leuven (OT 04/31; OT 08/023), the Flanders Fund for Scientific Research (project G.0603.08), and the Institute for the Promotion of Innovation by Science and Technology in Flanders (project IWT-050633) for financial support. QTH is a postdoctoral fellow of the Research Council of the KU Leuven.

Appendix

(Nomenclatur)

Parameter	
C_{CO_2}	CO_2 concentration (mol m^{-3})
$C^*_{CO_2}$	Equilibrium CO_2 concentration in liquid phase of outer membrane (mol m^{-3})
$C_{HCO_3^-}$	HCO_3^- concentration (mol m^{-3})
C_i	Concentration of gas i (mol m^{-3})
C_{O_2}	O_2 concentration (mol m^{-3})
$C^*_{O_2}$	Equilibrium O_2 concentration in liquid phase of outer membrane (mol m^{-3})
D_{CO_2}	CO_2 diffusivity (m^2 s^{-1})
$D_{CO_2,tissue}$	CO_2 apparent diffusivity of tissue (m^2 s^{-1})
$D_{HCO_3^-}$	HCO_3^- diffusivity (m^2 s^{-1})
D_i	Macroscopic apparent diffusivity of gas i (m^2 s^{-1})
D_{O_2}	O_2 diffusivity (m^2 s^{-1})
$D_{O_2,mem}$	O_2 diffusivity through cell membrane (m^2 s^{-1})
$E_{a,V_{m,O_2}}$	Activation energy of O_2 consumption (kJ mol^{-1})
$E_{a,V_{m,f,CO_2}}$	Activation energy of CO_2 production (kJ mol^{-1})
$h_{O_2,mem}$	O_2 permeability through cell membrane (m s^{-1})
$h_{CO_2,mem}$	CO_2 permeability through cell membrane (m s^{-1})
$h_{HCO_3^-,mem}$	HCO_3^- permeability through cell membrane (m s^{-1})
H_{O_2}	Henry's constant for O_2 (mol m^{-3} kPa^{-1})
H_{CO_2}	Henry's constant for CO_2 (mol m^{-3} kPa^{-1})
$[H^+]$	H^+ concentration (mol l^{-1})
J_{CO_2}	The flux of CO_2 (mol m^{-2} s^{-1})
J_{O_2}	The flux of O_2 (mol m^{-2} s^{-1})
k_i	CO_2 hydration velocity constant (s^{-1})
k_2	CO_2 dehydration velocity constant (s^{-1})
K	Permeation coefficient (m^2)
K_a	Acid dissociation constant for H_2CO_3 (mol l^{-1})
$K_{m,c}$	Michaelis–Menten constant for cytochrome *c* (μM)
K_{m,f,O_2}	Michaelis–Menten constant of O_2 inhibition on fermentative CO_2 production (mol m^{-3})
K_{mn,CO_2}	Michaelis–Menten constant for non-competitive CO_2 inhibition (mol m^{-3}).
K_{m,O_2}	Michaelis–Menten constant for O_2 consumption (mol m^{-3})
P	Total pressure (kPa)
$r_{q,ox}$	Respiration quotient
R	Universal gas constant (8.314 J mol^{-1} K^{-1})
R_i	Effective respiration term of the tissue (mol m^{-3} s^{-1})
R_{O_2}	O_2 consumption rate (mol m^{-3} s^{-1})
R_{CO_2}	CO_2 consumption rate (mol m^{-3} s^{-1})
T	Temperature (K)
t	Time (s)
$\mathbf{u}$	Velocity vector (m s^{-1})
V_{m,f,CO_2}	Maximal fermentative CO_2 production rate (mol m^{-3} s^{-1})
$V_{m,f,CO_2,ref}$	Maximal fermentative CO_2 production rate at reference temperature (mol m^{-3} s^{-1}).
V_{m,O_2}	Maximal O_2 consumption rate (mol m^{-3} s^{-1})
$V_{m,O_2,ref}$	Maximal O_2 consumption rate at reference temperature (mol m^{-3} s^{-1})
Symbols	
α_i	Gas capacity of the component i
μ	Viscosity (Pa.s)
ϵ	Porosity of tissue
∇	Gradient operator (m^{-1})
Δ	Difference
Subscripts	
g	Gas phase
i	O_2, CO_2 or N_2
l	liquid phase
r	Radial direction
w	Cell wall
z	Vertical axis
∞	Ambient atmosphere

References

Aalto T, Juurola E. 2002. A three-dimensional model of CO_2transport in airspaces and mesophyll cells of a silver birch leaf. *Plant, Cell and Environment* **25,** 1399–1409.

Agar T, Streif J, Bangerth F. 1997. Effect of high $CO_2$and controlled atmosphere (CA) on the ascorbic and dehydroascorbic acid content of some berry fruits. *Postharvest Biology and Technology* **11,** 45–55.

Beaudry RM. 1999. Effect of O_2 and CO_2 partial pressure on selected phenomena affecting fruit and vegetable quality. *Postharvest Biology and Technology* **15,** 293–303.

Blokhina OB, Chirkova TV, Fagerstedt KV. 2001. Anoxic stress leads to hydrogen peroxide formation in plant cells. *Journal of Experimental Botany* **52,** 1179–1190.

Borisjuk L, Rolletschek H. 2009. Oxygen status of developing seed. *New Phytologist* **182,** 17–30.

Boron WF. 2004. Regulation of intracellular pH. *Advances in Physiology Education* **28,** 160–179.

Chevillotte P. 1973. Relation between the reaction cytochrome oxidase—oxygen and oxygen uptake in cells *in vivo*. *Journal of Theoretical Biology* **39,** 277–295.

de Pablo JJ, Curtin WA. 2007. Multiscale modeling in advanced materials research: challenges, novel methods, and emerging applications. *MRS Bulletin–Material Research Society* **32,** 905–912.

Denison RF. 1992. Mathematical modeling of oxygen diffusion and respiration in legume root nodules. *Plant Physiology* **98,** 901–907.

Franck C, Baetens M, Lammertyn J, Verboven P, Nicolaï BM. 2003. Ascorbic acid content during fruit development and postharvest storage of conference pears. *Journal of Agriculture and Food Chemistry* **51,** 4757–4763.

Franck C, Lammertyn J, Ho QT, Verboven P, Verlinden B, Nicolaï BM. 2007. Browning disorders in pear: a review. *Postharvest Biology and Technology* **43,** 1–13.

Geigenberger P, Fernie AR, Gibon Y, Christ M, Stitt M. 2000. Metabolic activity decreases as an adaptive response to low internal oxygen in growing potato tubers. *Biological Chemistry* **381,** 723–740.

Gnaiger E. 2003. Oxygen conformance of cellular respiration: a perspective of mitochondrial physiology. *Advances in Experimental Medicine and Biology* **543,** 39–55.

Hertog M, Peppelenbos HW, Evelo RG, Tijskens LM. 1998. A dynamic and generic model on the gas exchange of respiring produce: the effects of oxygen, carbon dioxide and temperature. *Postharvest Biology and Technology* **14,** 335–349.

Ho QT, Verboven P, Mebatsion HK, Verlinden BE, Vandewalle S, Nicolaï BM. 2009. Microscale mechanisms of gas exchange in fruit tissue. *New Phytologist* **182,** 163–174.

Ho QT, Verlinden BE, Verboven P, Nicolaï BM. 2006*a*. Gas diffusion properties at different positions in the pear. *Postharvest Biology and Technology* **41,** 113–120.

Ho QT, Verlinden BE, Verboven P, Vandewalle S, Nicolaï BM. 2006*b*. A permeation–diffusion–reaction model of gas transport in cellular tissue of plant materials. *Journal of Experimental Botany* **57,** 4215–4224.

Ho QT, Verboven P, Verlinden BE, Lammertyn J, Vandewalle S, Nicolaï BM. 2008. A continuum model for gas exchange in pear fruit. *Plos Computational Biology* **4,** e1000023.

Kader AA. 1988. Respiration and gas exchange of vegetables. In: Weichmann J, ed. *Postharvest physiology of vegetables*. New York: Marcel Dekker Inc., 25–43.

Lammertyn J, Aerts M, Verlinden BE, Schotsmans W, Nicolaï BM. 2000. Logistic regression analysis of factors inuencing core breakdown in ' *Conference*' pears. *Postharvest Biology and Technology* **20,** 25–37.

Lammertyn J, Franck C, Verlinden BE, Nicolaï BM. 2001*b*. Comparative study of the O2, CO2, and temperature effect on respiration between 'Conference' pear cells in suspension and intact pears. *Journal of Experimental Botany* **52,** 1769–1777.

Lammertyn J, Scheerlinck N, Jancsók P, Verlinden BE, Nicolaï BM. 2003. A respiration–diffusion model for 'Conference' pears I: model development and validation. *Postharvest Biology and Technology* **30,** 29–42.

Lammertyn J, Scheerlinck N, Verlinden BE, Schotsmans W, Nicolaï BM. 2001. Simultaneous determination of oxygen diffusivity and respiration in pear skin and tissue. *Postharvest Biology and Technology* **23,** 93–104.

Larrigaudiere C, Lentheric I, Pinto E, Vendrell M. 2001. Short-term effects of air and controlled atmosphere storage on antioxidant metabolism in Conference pears. *Journal of Plant Physiology* **158,** 1015–1022.

Ludwig B, Bender E, Arnold S, Hüttemann M, Lee I, Kadenbach B. 2001. Cytochrome c oxidase and the regulation of oxidative phosphorylation. *Chembiochemistry* **2,** 392–403.

Mannapperuma JD, Singh RP, Montero ME. 1991. Simultaneous gas diffusion and chemical reaction in foods stored in modified atmospheres. *Journal of Food Engineering* **14,** 167–183.

Mebatsion HK, Verboven P, Ho QT, Mendoza F, Verlinden BE, Nguyen TA, Nicolaï BM. 2006. Modelling fruit microstructure using novel ellipse tessellation algorithm. *CMES–Computer Modeling in Engineering and Sciences* **14,** 1–14.

Mebatsion HK, Verboven P, Ho QT, Verlinden BE, Nicolaï BM. 2008. Modelling fruit micro structures, why and how? *Trends in Food Science and Technology* **19,** 59–66.

Mendoza F, Verboven P, Mebatsion HK, Kerckhofs G, Wevers M, Nicolaï BM. 2007. Three-dimensional pore space quantification of apple tissue using X-ray computed microtomography. *Planta* **226,** 559–570.

Millar AH, Bergersen FJ, Day DA. 1994. Oxygen affinity of terminal oxydases in soybean mitochondria. *Plant Physiology and Biochemistry* **32,** 847–852.

Morison JIL, Gallouet E, Lawson T, Cornic G, Herbin R, Baker NR. 2005. Lateral diffusion of CO_2 in leaves is not sufficient to support photosynthesis. *Plant Physiology* **139,** 254–266.

Nishi T, Forgac M. 2002. The vacuolar (H^+)-ATPases—Nature's most versatile proton pumps. *Nature Reviews Molecular Cell Biology* **3,** 94–103.

Parkhurst DF, Mott KA. 1990. Intercellular diffusion limits to CO_2 uptake in leaves: studies in air and helox. *Plant Physiology* **94,** 1024–1032.

Peppelenbos HW, van't Leven J. 1996. Evaluation of four types of inhibition for modeling the influence of carbon dioxide on oxygen consumption of fruits and vegetables. *Postharvest Biology and Technology* **7,** 27–40.

Raghavan P, Ghosh S. 2004. Adaptive multiscale computation modelling of composite materials. *CMES–Computer Modelling in Engineering and Sciences* **5,** 151–170.

Regenauer-Lieb K, Yuen DA. 2003. Modeling shear zones in geological and planetary sciences: solid- and fluid-thermal-mechanical approaches. *Earth-Science Reviews* **63,** 295–349.

Rolfe DFS, Brown GC. 1997. Cellular energy utilization and molecular origin of standard metabolic rate in mammals. *Physiological Reviews* **77,** 731–758.

Rolletschek H, Borisjuk L, Koschorreck M, Wobus U, Weber H. 2002. Legume embryos develop in a hypoxic environment. *Journal of Experimental Botany* **53,** 1099–1107.

Rolletschek H, Weber H, Borisjuk L. 2003. Energy status and its control on embryogenesis of legumes. Embryo photosynthesis contributes to oxygen supply and its coupled to biosynthetic fluxes. *Plant Physiology* **132,** 1196–1206.

Saquet AA, Streif J, Bangerth F. 2003. Energy metabolism and membrane lipid alterations in relation to brown heart development in Conference pears during delayed controlled atmoshpere storage. *Postharvest Biology Technology* **30,** 123–132.

Schotsmans W, Verlinden BE, Lammertyn J, Nicolaï BM. 2003. Simultaneous measurement of oxygen and carbon dioxide diffusivity in pear fruit tissue. *Postharvest Biology and Technology* **29,** 155–166.

Seymour RS. 2001. Diffusion pathway for oxygen into highly thermogenic florets of the arum lily Philodendron selloum. *Journal of Experimental Botany* **52,** 1465–1472.

Smith FA, Raven JA. 1979. Intracellular pH and its regulation. *Annual Review of Plant Physiology* **30,** 289–311.

Solomos T. 1982. Effect of low oxygen concentration on fruit respiration: nature of respiration diminution. In: Richardson DG, Meheriuk M, eds. *Control atmosphere for storage and transport of perishable agricultural commodities*. Beaverton: Timber Press, 171–179.

Taiz L, Zeiger E. 1993. *Plant physiology*. California: The Benjamin/Cummings Publishing Company Inc.

Veltman RH, Lentheric I, Van der Plas LHW, Peppelenbos HW. 2003. Browning in pear fruit (*Pyrus communis* L. cv Conference) may be a result of a limited availability of energy and antioxidants. *Postharvest Biology and Technology* **28,** 295–302.

Veltman RH, Sanders MG, Persijn ST, Peppelenbos HW, Oosterhaven J. 1999. Decreased ascorbic acid levels and brown core development in pears (*Pyrus communis* L. cv. Conference). *Physiology Plantarum* **107,** 39–45.

Verboven P, Kerckhofs G, Mebatsion HK, Ho QT, Temst K, Wevers M, Cloetens P, Nicolaï BM. 2008. 3-D gas exchange pathways in pome fruit characterised by synchrotron X-ray computed tomography. *Plant Physiology* **47,** 518–527.

Warren CR. 2008. Soil water deficits decrease the internal conductance to CO_2 transfer but atmospheric water deficits do not. *Journal of Experimental Botany* **59,** 327–334.

Wood BD, Quintard M, Whitaker S. 2002. Calculation of effective diffusivities for biofilms and tissues. *Biotechnology and Bioengineering* **77,** 495–516.